1997

Numerical Computation of Flapping-Wing Propulsion and Power Extraction

Jones, K.D.

Jones, K.D. and Platzer, M.F., "Numerical Computation of Flapping-Wing Propulsion and Power Extraction," AIAA Paper No. 97-0826, 35th AIAA Aerospace Sciences Meeting, Reno, Nevada,

AIAA−97−0826
NUMERICAL COMPUTATION OF FLAPPING−WING PROPULSION AND POWER EXTRACTION

K.D.Jones and M.F.Platzer
Naval Postgraduate School
Monterey, CA

35th Aerospace Sciences Meeting & Exhibit
January 6−10, 1997 / Reno, NV

NUMERICAL COMPUTATION OF FLAPPING-WING PROPULSION AND POWER EXTRACTION

K. D. Jones† and M. F. Platzer‡

Naval Postgraduate School
Monterey, California

Abstract

Numerical procedures are presented for the systematic computation of unsteady flows over moving airfoils or airfoil combinations, and these procedures are applied to the investigation of flapping-wing propulsion and power extraction. Flow solutions about single foils are computed using an unsteady, two-dimensional panel code coupled with a boundary layer algorithm and driven using an interactive graphical user interface. Flow solutions about airfoil combinations are computed using a companion, multi-element version of the panel code.

Results for pitching-only and plunging-only motions compare favorably with theory and reasonably well with experimental results. Extensive computations are performed over the broad parameter space for combined pitching and plunging motions using the foil as both a propulsive device and as a wingmill or power-extraction device. Results modeling flight in ground effect are compared with other numerical and experimental results.

Nomenclature

c = chord length
C_d = drag coefficient per unit span, $D/(q_\infty c)$
C_l = lift coefficient per unit span, $L/(q_\infty c)$
C_m = moment coefficient per unit span, $M/(q_\infty c^2)$
C_p = power coefficient per unit span, $-C_l\dot{y} - C_m\dot{\alpha}$
C_t = thrust coefficient per unit span, $T/(q_\infty c)$
D = drag per unit span
f = frequency in Hertz
h = plunge amplitude in terms of c
k = reduced frequency, $\omega c/V_\infty$
L = lift per unit span
M = moment per unit span
q_∞ = freestream dynamic pressure, $1/2\rho_\infty V_\infty^2$
R_L = chord Reynolds number, $V_\infty c/\nu_\infty$
S_t = Strouhal number, $\omega hc/V_\infty$
t = time
T = thrust per unit span $(-D)$
V_p = maximum plunge velocity, hk $(= S_t)$
V_∞ = freestream velocity
x_p = pivot location from LE in terms of c
α = angle of attack
$\Delta\alpha$ = pitch amplitude in degrees
ϕ = phase between pitch and plunge
η = propulsive efficiency, C_t/C_p
λ = wake wavelength in terms of c
ν_∞ = freestream kinematic viscosity
ω = circular frequency
ρ_∞ = freestream density
τ = nondimensional time, tV_∞/c
$(\dot{})$ = rate of change w.r.t. τ

Introduction

The first explanations of thrust production from flapping wings were given in 1909 by Knoller[1] and independently a few years later by Betz.[2] The Knoller-Betz effect was experimentally verified by Katzmayr[3] in 1922 for fixed airfoils in an oscillatory flowfield. Birnbaum,[4,5] in 1924 and 1925, investigated the unsteady motion of airfoils both aeroelastically, measuring the conditions leading to flutter, and as a propulsive device.

In 1935, Von Kármán and Burgers[6] offered the first theoretical explanation of drag or thrust production based on the resulting vortex street (i.e., the placement and orientation of the wake vortex elements). Vortex streets characteristic of drag production (e.g. a Karman vortex street behind a cylinder) have a row of vortices of clockwise rotation above the symmetry plane, and a row of vortices of counter-clockwise rotation below the symmetry plane, with the flow going from left to right, as shown in Fig. 1 for an airfoil plunging at a low Strouhal number ($k = 3.6$, $h = 0.08$, $S_t = 0.29$). The vortices induce a velocity or momentum deficit on the centerline indicative of drag, and the wake wavelength, λ, defined here as the distance between vortex centers of same rotation, is shorter than the wavelength predicted by linear theory, $\lambda_{l.t.} = 2\pi/k$, due to the production of drag.

† NRC Research Associate, Member, AIAA

‡ Professor, Associate Fellow, AIAA

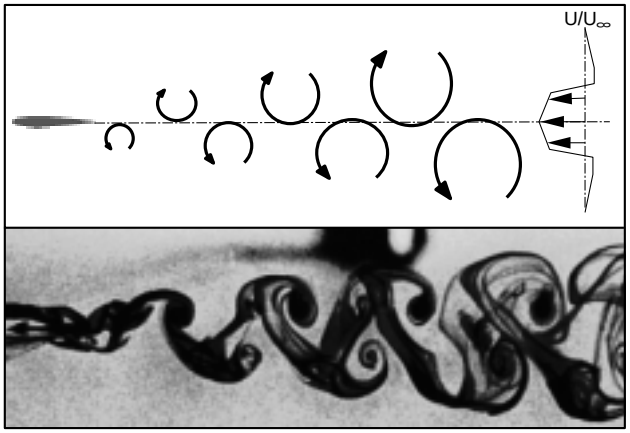

Fig. 1: Drag producing vortex street.[7]

Oscillating the airfoil more energetically the vortex street shown in Fig. 2 is generated ($k = 3.0$, $h = 0.20$, $S_t = 0.60$).

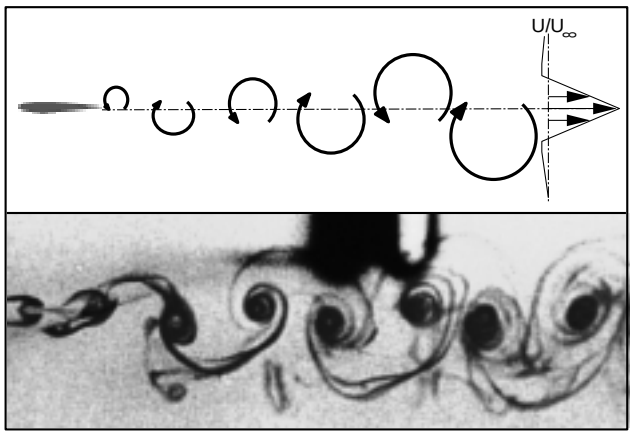

Fig. 2: Thrust producing vortex street.[7]

Here the upper row of vortices rotates counterclockwise, and the lower row rotates clockwise. Now the vortices induce a velocity or momentum surplus on the centerline, and the wake wavelength is longer than that predicted by linear theory. (Note, the reduced frequency in the first case is higher than in the second case; evidence that the Strouhal number, not the reduced frequency, is the defining parameter in these wake dominated flows).

In 1936, Garrick[8] extended the compact formulations of Theodorsen[9] to compute the longitudinal force for pitching and/or plunging airfoils. Garrick showed that in inviscid, incompressible flow a positive thrust is generated for all pure plunging motions with propulsive efficiencies approaching unity as the frequency approaches zero and reducing asymptotically to 50 percent at high frequencies. However, Garrick also found that the thrust is roughly proportional to the square of the frequency. Thus, at low frequencies, where high propulsive efficiencies are obtained, low thrust coefficients are produced. This implies that large flapping wings would be needed in order to achieve significant thrust at high efficiency. Furthermore, as indicated in Fig. 1, at low Strouhal numbers, drag, not thrust, is produced due to flow viscosity, indicating that inviscid thrust predictions in the low frequency range are likely to be far too optimistic.

It was recognized that at reasonable frequencies a large portion of the energy used to flap the airfoil was lost in the form of vorticity shed in the wake. Most researchers lost interest in flapping wings as a replacement for conventional propellers; however, in 1942 Schmidt[10] discovered a method for recovering much of the vortical energy released from a flapping airfoil. He demonstrated that additional thrust could be generated by placing a stationary airfoil in the oscillatory wake of a flapping airfoil. Katzmayr[3] had previously shown that a stationary airfoil in an oscillatory flow produced thrust, and Schmidt noted that the stationary airfoil in the oscillatory wake required no additional power input; thus, the propulsive efficiency of the system could be increased substantially over a broad frequency range.

Obvious mechanical difficulties arise from pure plunging motions, and Schmidt addressed this difficulty by developing his *wave propeller*, shown in Fig. 3, where the lead airfoil is moved in a circular path with a fixed angle of attack creating an oscillating flowfield for the second airfoil.

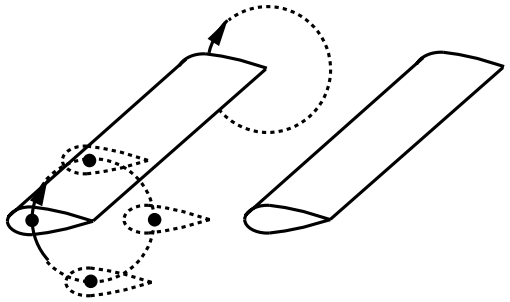

Fig. 3: The Schmidt *wave propeller*.

Schmidt demonstrated his wave propeller on a catamaran boat and claimed propulsive efficiencies comparable to those obtained with conventional propellers.

In 1977, Bosch[11] developed a linear theory for predicting propulsion from flapping airfoils and airfoil combinations, for the first time including wake interference effects in propulsive efficiency computations, and in 1982 DeLaurier and Harris[12] obtained experimental measurements of flapping-wing propulsion.

Thrust production due to pitching motions was experimentally demonstrated by Koochesfahani[13] in 1989. Unlike plunging foils, which produce thrust for

all frequencies, pitching foils produce drag for very low frequencies, a feature that leads to pitch-instability or flutter. In the case of flutter, energy is extracted from the flow, creating a drag profile in the wake of the foil and amplifying the motion of the foil.

Energy-extraction from an airfoil undergoing pitching flutter is rather benign, that is, the pitch-amplitude growth rate is small, as shown in Jones and Platzer.[14] This is not the case for airfoils undergoing coupled pitching and plunging motions, where energy extraction and/or aeroelastic-motion growth rates can be very high. The use of a two-degree-of-freedom fluttering airfoil as a windmill was proposed by McKinney and DeLaurier.[15] They built a model *wingmill* and in a windtunnel showed that power generation efficiencies were competitive with other windmill designs.

More recently, the problem of flapping foil propulsion has been considered by Liu[16,17] using vortex lattice and panel methods, by Send[18,19] using linearized theory and by Hall and Hall[41] using vortex lattice methods.

In the present study comparisons are performed with these past, single-mode studies (i.e., pitching or plunging motions), and extensive investigations of the dual-mode parameter space including both thrust production and energy extraction are made. The effects of the nonlinear, deforming wake model, airfoil geometry and flow viscosity are also evaluated. These investigations are extended to a two airfoil system, modeling an airfoil in ground effect, and simulations are made regarding the production of thrust near a ground plane.

Approach

The numerical methods utilized in this study are briefly described here, with details of the algorithms given in the cited references.

Panel Code Flow solutions are computed using an unsteady, potential-flow code originally developed by Teng,[20] with a Graphical User Interface (GUI) developed by Jones and Center[21] and additional modifications discussed here.

The basic, steady panel code follows the approach of Hess and Smith,[22] where the airfoil is approximated by a finite number of panels, each with a local, uniform, distributed source strength and all with a global, uniform, distributed vorticity strength. For n panels there are n unknown source strengths, q_j, and an unknown vorticity strength, γ. Boundary conditions include flow tangency at the midpoint of the n panels and the Kutta condition which postulates that the pressure on the upper and lower surfaces of the airfoil at the trailing edge must be equal.

The unsteady panel code adopts the procedure of Basu and Hancock,[23] where a wake panel is attached to the trailing edge through which vorticity is shed into the flow. The Helmholtz theorem states that the bound vorticity in a flow remains constant, thus a change in circulation about the airfoil must result in the release of vorticity into the wake equal in magnitude and opposite in direction, given numerically by

$$\Delta_k(\gamma_w)_k + \Gamma_k = \Gamma_{k-1} \tag{1}$$

where Δ is the wake panel length, γ_w is the distributed vorticity strength on the wake panel and Γ is the circulation about the airfoil, and where the subscript k indicates the current time step, and $k-1$ indicates the previous time step.

The wake panel introduces two additional unknowns; the wake panel length and its orientation, θ_k. Thus, two additional conditions must be specified for closure;

1. The wake panel is oriented in the direction of the local resultant velocity at the panel midpoint.
2. The length of the wake panel is proportional to the magnitude of the local resultant velocity at the panel midpoint and the time-step size.

The essential elements of this scheme are summarized in Fig. 4.

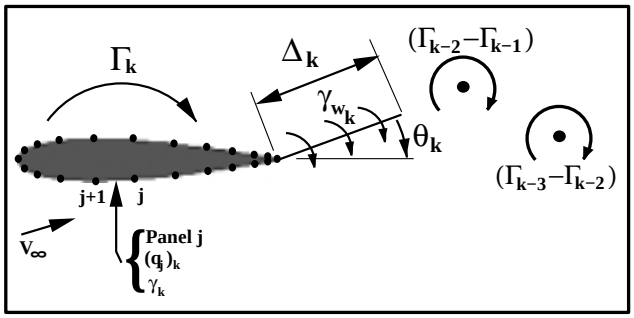

Fig. 4: Schematic of the panel code wake model.

At the end of each time step the vorticity contained in the wake panel is concentrated into a point vortex which is shed into the wake and convected downstream with the flow, influencing and being influenced by the other shed vortices and the airfoil. Note, implementation of this approach requires an iterative scheme, since the velocity direction and magnitude used to define the wake panel are not initially known. Note also that this wake model is nonlinear. The unsteady panel code has been extensively documented in Refs. 7, 14, 21 and 24-28.

Boundary Layer Code Flow properties in the boundary layer are computed using the Keller-Cebeci box method.[29] The code was generated and combined with a steady panel code by Nowak.[30] The general

algorithm and several modifications used in the current implementation are discussed below.

The boundary layer code treats the airfoil surface as a flat plate with a variable pressure gradient, and steady conditions are assumed within the boundary layer. Laminar, transitional and turbulent regions are considered, and the turbulent region is computed using the Cebeci-Smith (CS) eddy-viscosity model. Like all eddy-viscosity methods, the CS model leaves the basic boundary layer equations unchanged but modifies the viscosity term by adding a local eddy viscosity, $\nu = \nu_\infty + \epsilon_m$. The CS model divides the viscous region into an inner and an outer layer with the eddy viscosity in each region empirically formulated. The inner region is modeled by

$$\left(\frac{\epsilon_m}{\nu}\right)_i = 0.16\sqrt{Re_x}\Big[1-\exp(-y/A)\Big]^2\eta^2\nu_\infty\gamma_{tr}\ , \quad (2)$$

and the outer region is modeled by

$$\left(\frac{\epsilon_m}{\nu}\right)_o = 0.0168\sqrt{Re_x}\Big[\eta_e - f_e\Big]\gamma_{tr}\ , \quad (3)$$

where

$$Re_x = \frac{U_e}{V_\infty}\xi R_L\ , \quad (4)$$

$$\frac{y}{A} = \frac{\eta}{26}\sqrt[4]{Re_x}\sqrt{\nu_w}\ , \quad (5)$$

and where ξ, η and f are the Falkner-Skan variables. The term γ_{tr} models the length of the transition or intermittency region, and its formulation is discussed below.

For the steady implementation of the code developed by Nowak the transition point is specified as input, presumably determined from experimental data. This is of little use in the present unsteady approach, as transition points would need to be specified for an infinite variety of conditions. Thus, Michel's criterion is used to predict transition onset, where transition is initiated when the Reynolds number based on momentum thickness, $R_\theta = U_e\theta/\nu_\infty$, and the Reynolds number based on x, Re_x, satisfy the equation

$$R_{\theta_{tr}} = 1.174\left(1+\frac{22,400}{Re_{x_{tr}}}\right)Re_{x_{tr}}^{0.46}\ . \quad (6)$$

The Chen-Thyson intermittency model is used to predict the transition length where

$$\gamma_{tr} = 1-\exp\left[-G(x-x_{tr})\int_{x_{tr}}^{x}\frac{1}{U_e}dx\right] \quad (7)$$

and

$$G = \frac{1}{G_{tr}}\left(\frac{U_e}{V_\infty}\right)^3 R_L^2 Re_{x_{tr}}^{-1.34}\ . \quad (8)$$

In the original Chen-Thyson formulation G_{tr} is set to a constant value of 1200, but in the present implementation it is given by Cebeci[31] as a function of the transition Reynolds number

$$G_{tr} = 71\Big[\ln(Re_{x_{tr}}) - 4.732\Big]\ . \quad (9)$$

Note, while the boundary layer routine is steady, it has been shown that, for low reduced frequencies, changes in the boundary layer occur much more quickly than changes in the external flow, thus a steady boundary layer analysis is sufficient.

The boundary layer code produces skin-friction results up to the point of separation which may be used to estimate viscous drag. However, merely summing the drag components due to the integrated surface pressure from the panel code and the skin-friction from the boundary layer code yields a rather poor prediction of the complete profile drag, due to momentum loss within the boundary layer, pressure errors in the separated region and other effects. Thus, the Squire-Young empirical relation is used to predict the airfoil profile drag. The Squire-Young formula, as given by Cebeci and Smith,[32] is

$$C_d = \left[2\left(\frac{\theta}{c}\right)\left(\frac{U_e}{V_\infty}\right)\exp\Big[0.5(H+5)\Big]\right]_{TE}\ . \quad (10)$$

which uses the momentum thickness, θ, and the shape factor, $H = \delta^*/\theta$, along with the external velocity, U_e, at the trailing edge (TE) to predict the total (steady) drag. In practice, the formula may not be applied at the TE, since the panel code requires produces highly adverse pressure gradient near the trailing edge forcing the flow to separate. As suggested in Ref. 32, the formula is applied slightly ahead of the predicted separation point. A drag polar predicted by the present approach is compared to the experimental results of Abbott and von Doenhoff[33] in Fig. 5 for a NACA 0012 with a chord-Reynolds number of 6 million.

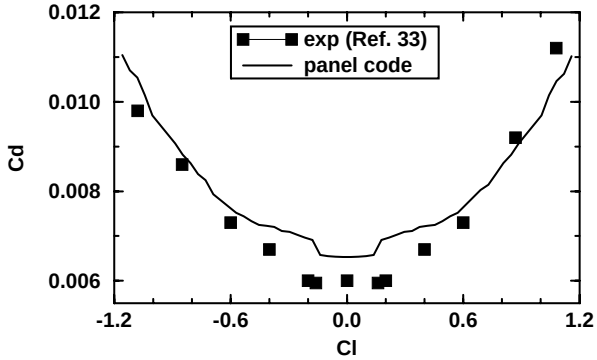

Fig. 5: Drag polar comparison.

Two-foil Code The panel method described above was extended to multiple airfoil systems by Pang.[34] The approach is similar to the single airfoil code, but flow-tangency and Kutta-condition boundary conditions must be solved simultaneously for the full system. Details of the algorithm are given in Ref. 29. The airfoils may be arbitrarily sized and placed in the flowfield, and the motions of each may be individually defined. The two-foil code is validated in Refs. 14, 24-26, 28 and 34.

Configurations Three general configurations are used for the simulations performed here. The configuration schematics and parameter definitions for them are illustrated in Figs. 6a-c.

The single airfoil case is shown in Fig. 6a. The airfoil shape is arbitrary and has a chord length of 1. The pivot point (elastic axis) is located at x_p, measured positive from the leading edge toward the trailing edge.

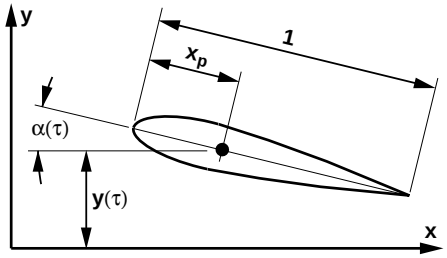

Fig. 6a: Single airfoil schematic.

The angle of attack (AOA) and plunge displacement are time-dependent, and are given in the present study by

$$\alpha(\tau) = \alpha_0 + \Delta\alpha \cos(k\tau) \ , \tag{11}$$

and

$$y(\tau) = h_0 - h \cos(k\tau + \phi) \ , \tag{12}$$

respectively, where ϕ is the phase angle between the two modes. The flow direction is aligned with the positive x-axis and the plunge direction is aligned with the y-axis. Note, throughout this paper single-mode motions will be referred to as *pitching* or *plunging*, whereas the term *flapping* will imply a general combination of pitching and plunging.

The two airfoil system is shown in Fig. 6b. Each airfoil has the same degrees-of-freedom as the single-foil case, but the second foil may have a different chord length, and it is displaced from the first foil by x_0 and y_0, as shown. Note that $h_0 = y_0$ in Eq. (12).

A special case is shown in Fig. 6c, using the two-foil system to simulate an airfoil in ground effect. Recall that in potential flow the effect of a ground plane may be computed by placing mirror-image singularities within the ground-plane, as illustrated in the figure. Here the motion of the image airfoil must be the reciprocal of the motion of the real airfoil, and the wake generated by the image airfoil should be a mirror image of the wake generated by the real foil. The average height above the ground plane is given by h_0.

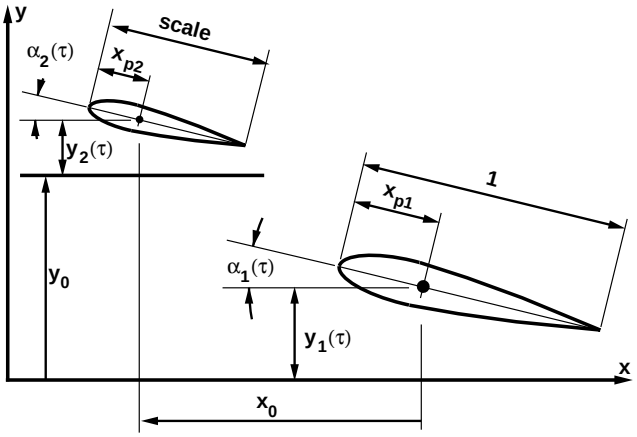

Fig. 6b: Two airfoil system.

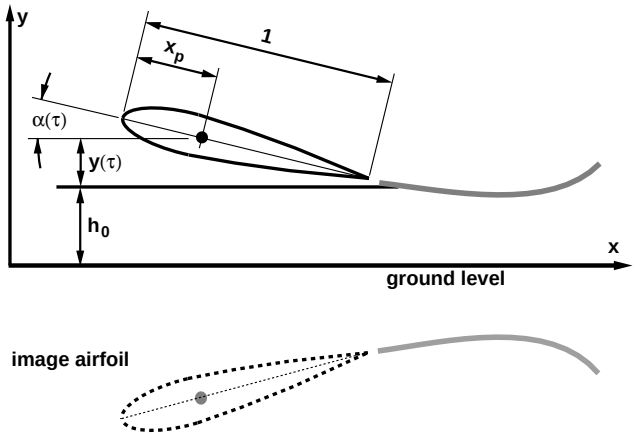

Fig. 6c: Airfoil in ground effect.

Results

In order to demonstrate the validity of the panel code (UPOT), results are presented with comparisons to theory and experimental studies. Unless otherwise noted, presented results from the panel code do not include viscous effects.

Many of the presented results include the propulsive efficiency, η. The common definition for thrust producing systems is

$$\eta = \frac{TV_\infty}{\dot{W}} \ , \tag{13}$$

where T is the thrust and $\dot{W}$ is the rate-of-work (power) input. In nondimensional terms this reduces to

$$\eta = \frac{C_t}{C_p} \ , \tag{14}$$

as shown in the nomenclature. The ideal propulsive efficiency is 1, meaning that the energy extracted in the form of thrust is equivalent to the energy needed to flap the airfoil, i.e., there are no losses. Negative values of η occur when drag is produced but work is still required to move the airfoil.

In cases where work is extracted from the flow (i.e., flutter or the *wingmill*), it is common to invert the definition of η, such that the ideal power-extraction efficiency is again 1 with lower values indicating that more energy is lost to drag than the energy extracted. This definition is not used here, however, as the dual definition of η might cause confusion. Thus, in cases where power is extracted from the flow, values of η will be greater than 1, with the ideal *wingmill* efficiency approaching $\eta = 1$ from above. Note, the definition of η is singular at $C_p = 0$, with one branch always less than 1, and the other branch always greater than 1. This is visible in several of the following figures.

Plunging The linear approach of Bosch[11] considers a flat-plate airfoil plunging with infinitesimal amplitude, at a specified frequency and with a nondeforming, planar wake. Numerical restrictions prevent UPOT from using a flat-plate airfoil, however, as shown in Fig. 7, the airfoil thickness has very little effect on the computed propulsive efficiency. Additionally, infinitesimal plunge amplitudes are not possible with UPOT, as the wake singularities may not be sufficiently resolved by the computer accuracy; thus, a value of $h = 0.1$ is used in Fig. 7.

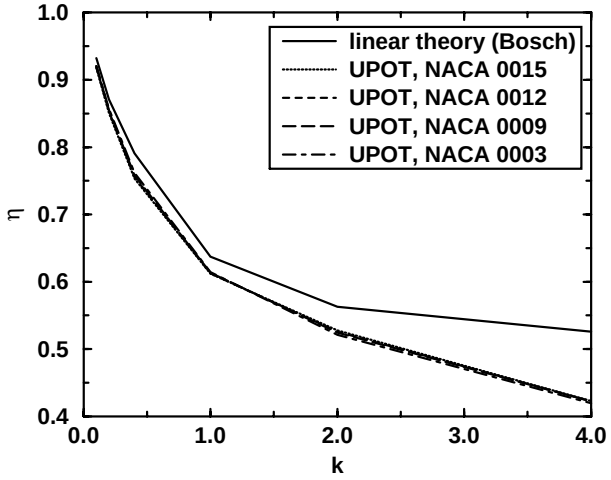

Fig. 7: Effect of airfoil thickness on η.

The agreement is good for small k but diminishes as k is increased. As will be shown, this is primarily due to the non-linear wake generated by UPOT. At high k the wake-deformation (i.e., vortex roll-up) becomes quite severe, showing up as a loss in propulsive efficiency.

In Fig. 8 the plunge amplitude is varied for a NACA 0012 airfoil, and it is clear that the plunge amplitude has a strong influence on the propulsive efficiency; efficiency diminishing with increased plunge amplitude. Again, the agreement with linear theory is quite good at low frequencies but diminishes as the frequency and plunge amplitude increase, reinforcing the argument that wake roll-up leads to a loss in efficiency.

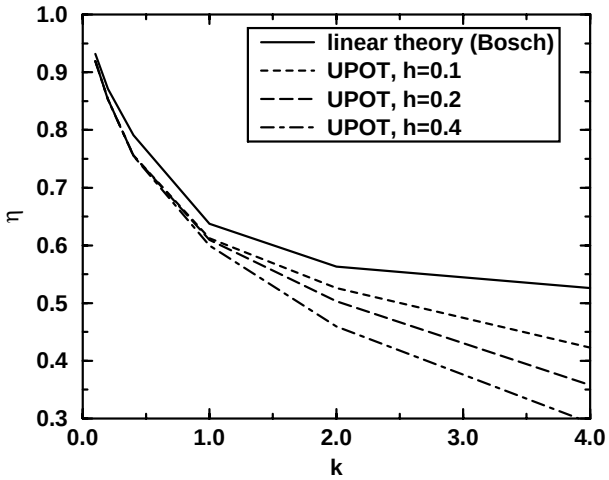

Fig. 8: Effect of plunge amplitude on η.

The linear approach of Garrick[4] allows for finite plunge amplitudes, but still assumes a non-deforming, planar wake. For plunging motions Garrick gives the thrust coefficient formulation

$$C_t = 4\pi k^2 h^2 (F^2 + G^2) \tag{15}$$

where F and G are the real and imaginary parts of the Theodorsen lift deficiency function, respectively, given in Table 1 as functions of k.

Table 1: Theodorsen lift deficiency function.

k	F	G
0.01	0.9824	-.0482
0.05	0.9090	-.1305
0.10	0.8320	-.1723
0.50	0.5979	-.1507
1.00	0.5394	-.1003
2.00	0.5129	-.0577
4.00	0.5037	-.0305
10.00	0.5006	-.0124

In Fig. 9 the thrust coefficient predicted by Garrick, is compared to the values computed with the panel code for a NACA 0012 airfoil for various reduced frequencies and plunge amplitudes. The agreement is good at lower values of h and k, or more appropriately, at lower values of the plunge velocity, $V_p = hk$, as introduced by Jones et al.[7] (Note, V_p has the form of

the Strouhal number with the plunge amplitude used as the length scale, $S_t = \omega hc/V_\infty$.) The panel code predicts a higher C_t than linear theory at high values of V_p. As will be shown, an increase in C_t often corresponds to a decrease in η.

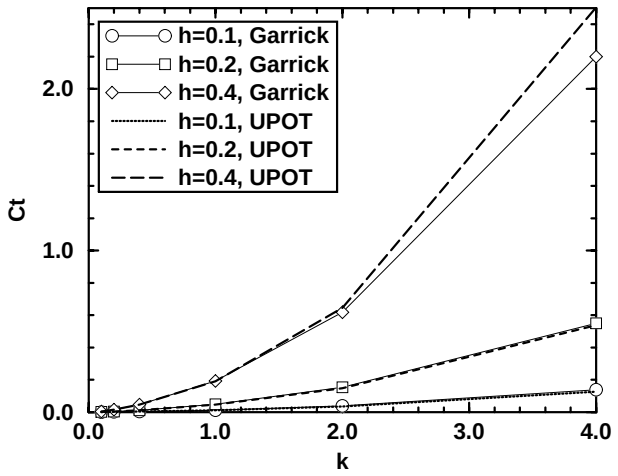

Fig. 9: Effect of plunge amplitude on C_t.

Several modifications were made to UPOT in order to investigate the effect of wake non-linearity. The first modification shuts off the wake deformation such that the individual wake elements convect downstream undisturbed, resulting in a sinusoidal wake of fixed wavelength and amplitude. The second modification restricts all the wake vorticity to the plane of the airfoil as it is in linear theory. Sample results are shown in Table 2 for a plunging NACA 0012 at $k = 4$, with the subscripts d, n and p denoting the deforming, non-deforming and planar wake models, respectively.

Table 2: C_t and η versus wake model

method	h	C_t	η
UPOT_d	0.1	0.125	0.441
UPOT_n	0.1	0.127	0.470
UPOT_p	0.1	0.134	0.519
linear theory	0.1	0.137	0.526
UPOT_d	0.4	2.50	0.293
UPOT_n	0.4	2.38	0.304
UPOT_p	0.4	2.13	0.519
linear theory	0.4	2.20	0.526

The remarkable agreement between linear theory and UPOT with the planar wake model demonstrates that the primary degradation of linear theory at higher Strouhal numbers is due to the inability of linear theory to consider out-of-plane vorticity. The use of a thick airfoil and discrete panels makes little difference in comparison.

Referring back to Fig. 2 an interesting observation may be made. As pointed out by Von Kármán and Burgers[6], the separated rows of vortices induce a velocity surplus along the centerline indicative of thrust production. However, these same vortices induce a streamwise force on the airfoil itself, and it can easily be seen in Fig. 2 that this will be a drag component. These induced forces are inversely proportional to the distance between the airfoil and the vortex element. In the deforming wake model the discrete wake elements roll up into large eddies, and these eddies convect downstream faster than the non-deforming wake. Thus, the induced drag effect of these eddies diminishes more quickly than the non-deforming wake model resulting in the higher C_t prediction shown in Tab. 2. However, the shed vorticity also provides a cross-stream force, that through most of the cycle reduces the power needed to plunge the foil. Thus, the airfoil with the deforming wake requires a greater power input and, hence, operates at a lower propulsive efficiency.

Unfortunately, this argument does not hold for the planar wake model. If the wake vorticity is confined to a plane coincident with the airfoil, then the discrete vortices can induce no streamwise influence on the airfoil. Additionally, the time-averaged velocity or momentum profiles downstream of the airfoil will show no deficit or surplus.

The Strouhal number is generally considered to be the defining parameter in wake dominated flows. For example, in Ref. 7 the wake structures behind a plunging foil were photographed, measured and classified for a wide range of reduced frequencies and plunge amplitudes. It was found that there are four basic types of vortical arrangements behind plunging airfoils. The first type is the drag producing case shown in Fig. 1, the third is the thrust producing case shown in Fig. 2, the second is actually the fine line between those two, where all the vortices lie on the centerline, and neither drag nor thrust is produced, and the fourth is a highly non-linear case where a deflected wake is formed. The fourth case occurs at relatively high Strouhal numbers ($St > 1$), and the resulting wake produces both an average thrust and lift.

In Fig. 10 the photographed wakes of Ref. 7 are classified according to the observed vortex positions. Lines of constant St are included demonstrating the approximate dependence of the experimental data on the Strouhal number. In contrast, Triantafyllou et al[35] classify the experimental results of Ohashi and Ishikawa[36] and Kadlec and Davis[37] which seem to show a slightly skewed dependence on h and k. The two thick, solid lines in Fig. 10 are taken from Ref. 35 and are curve-fit boundaries between the type 1,2 and 3 wake topologies based on the experimental data

of Refs. 36 and 37. The type 4, deflected wake topology was apparently not observed in any of the cited references other than Ref. 7 where they were duplicated experimentally and numerically and were found to be highly reproducible. It's important to note that these classifications are based purely on visual observations of the unsteady vortex structures. More quantitative experimental measurements as well as the panel / boundary-layer code suggest that these classifications are fairly conservative, with thrust generation occurring at Strouhal numbers as low as 0.1.

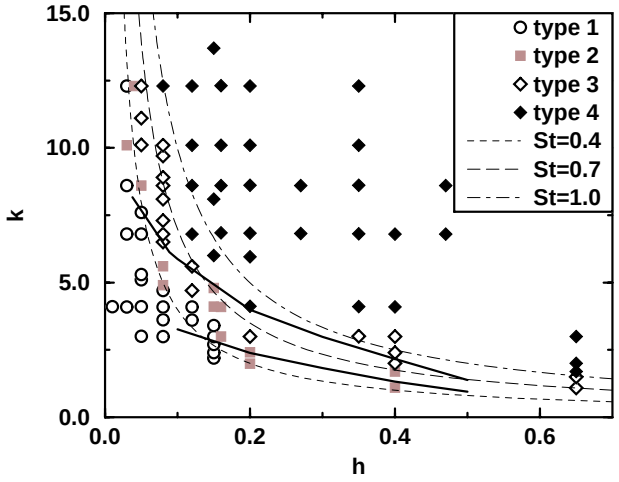

Fig. 10: Experimental wake structure classification.

The panel code cannot generate type 1 or 2 wakes, as they are a direct result of fluid viscosity. While the boundary between type 3 and 4 wakes cannot be determined with any great precision, it appears to be essentially a function of the Strouhal number. However, the computed thrust coefficient and propulsive efficiency do not demonstrate such a dependence on St. This is investigated by comparing results for cases with the same Strouhal number but different reduced frequencies and plunge amplitudes (i.e., hk =constant= 0.1).

The wakes generated for a NACA 0012 airfoil plunging with $k = 10$ and $h = 0.01$ in the upper plot, $k = 1$ and $h = 0.10$ in the middle plot and $k = 0.1$ and $h = 1.0$ in the lower plot are shown in Fig. 11a. The scale of the plots is adjusted to match the theoretical wake wavelengths, $\lambda = 2\pi/k$ (indicated by the vertical lines in the plots). The three plots have the same V_p and, hence, the same maximum induced α ($\alpha_i = 5.7$ degrees), but the wake non-linearity or instability (vortex roll-up) is much more pronounced at higher k. Intuition might suggest that the greater instability would indicate a greater thrust; however, this is not the case. As shown in Fig. 11b, for increasing plunge amplitude and decreasing reduced frequency with the Strouhal number fixed, both the production of thrust and the propulsive efficiency increase. This provides further evidence that the wake vorticity acts to diminish the propulsive efficiency. As the plunge amplitude is increased and the reduced frequency is decreased the wake vorticity is situated further from the airfoil and, hence, the negative effect is reduced.

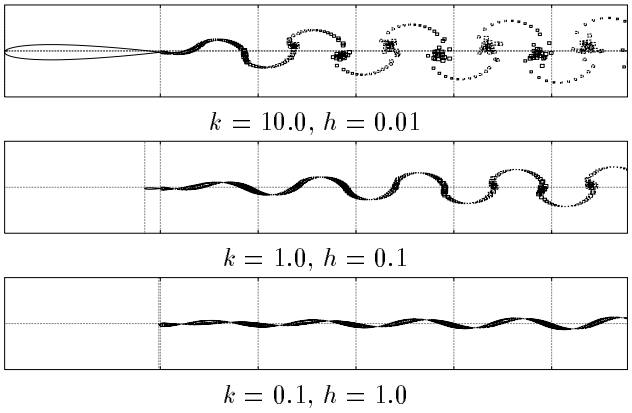

Fig. 11a: Dependence of wake instability on k.

In the extreme, if the airfoil is plunged at a constant velocity ($V_p = 0.1$), the propulsive efficiency goes to unity, and C_t and C_p are equal with C_t at a maximum value of 0.068. Of course, plunging with a constant velocity releases no vorticity into the wake, as this corresponds to steady flow at a constant angle of attack.

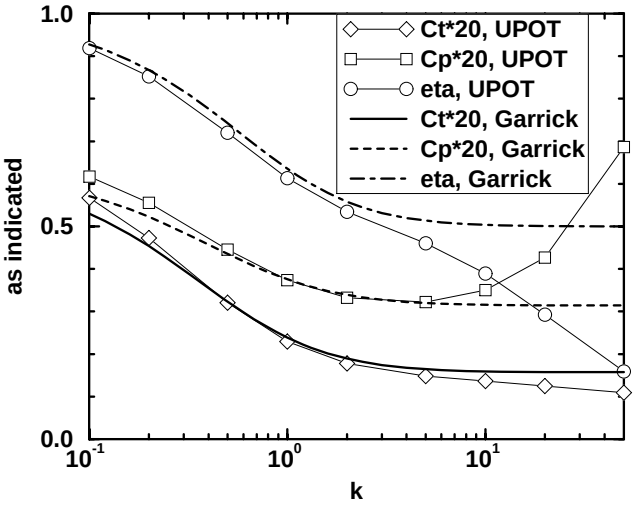

Fig. 11b: Thrust performance for constant $St = 0.1$.

This seems to be in agreement with observations of nature. High endurance sea birds generally have large spans, flap at low reduced frequencies and relatively large amplitudes (in terms of chordlengths).

In Fig. 11c the computed velocity profiles in the wake of the cases shown in Fig. 11a are plotted. The profiles are measured one wake-wavelength downstream of the trailing edge and are time-averaged values.

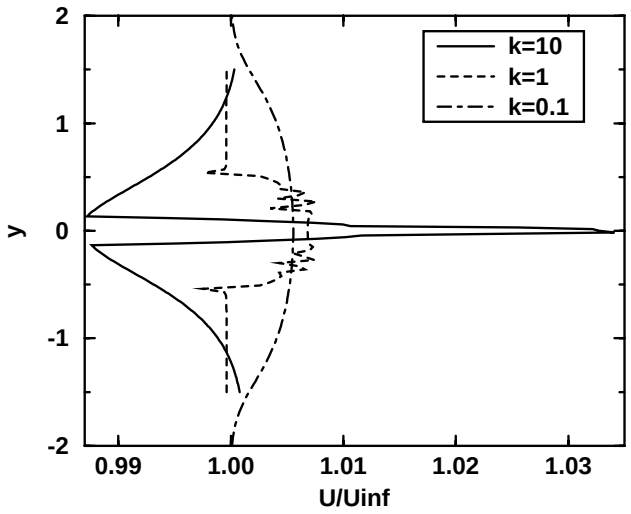

Fig. 11c: Velocity profile dependence on k.

Not surprisingly, the cases yielding a greater performance have a lower peak velocity and a more distributed profile. It has been suggested that optimal propulsive efficiency will occur when the velocity distribution in the wake most closely resembles the square velocity distribution behind an actuator disc. The results shown in Fig. 11c seem to be in partial agreement with this. However, the profile for $k = 1$ appears to be roughly square, but that case is not nearly as efficient as the case at $k = 0.1$ and, as discussed above, the extreme case of plunging with a constant velocity produces a roughly anti-symmetric profile.

Triantafyllou and Triantafyllou[38] claim that optimal performance arises from the proper location of wake vortices and an efficient jet profile in the wake, but according to Schmidt,[10] and from the evidence provided here, it seems that optimal performance occurs when the wake vorticity is minimized and/or located far from the airfoil, resulting in very weak or distributed jet profiles in the wake. Triantafyllou et al[35] claim that at Strouhal numbers greater than about 1 (based on the present definition of St) there is a decline in both the vortical convection speed and C_t. While it is possible that such a decline in thrust production may result from massive flow separation, a feature prohibited in the panel code, the panel code clearly demonstrates a lack of dependence of C_t, η and the vortical convection speed on St.

One further consideration that cannot easily be investigated by the present approach is dynamic stall. An airfoil plunging sinusoidally will have an induced angle of attack that may greatly exceed the static stall angle. At higher reduced frequencies stall may be delayed or prevented due to the dynamic pressure lag, but at the lower frequencies the airfoil may stall resulting in separated flow and a loss in performance over part of the oscillation cycle. The maximum induced angle of attack in the cases included in Figs. 11a-c, however, is just 5.7 degrees, well below the static stall angle of a NACA 0012.

Pitching Experimental thrust measurements for an airfoil pitching about the quarter chord were made by Koochesfahani[13] and are compared with Garrick's linear theory and the panel code for a NACA 0012 airfoil pitching in with $\Delta\alpha = 2$ degrees in Fig. 12.

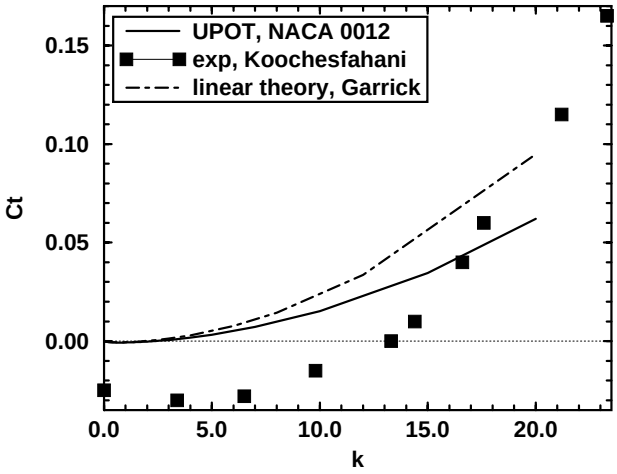

Fig. 12: Thrust production for pitching airfoils.

Note, the thrust formulation given by Garrick in Ref. 8 for pitching airfoils is incorrect. The correct formulation is given by Garrick in Ref. 39 as

$$C_t = \pi k^2 \Delta\alpha^2 \left[\left(F^2 + G^2\right) \left(\frac{1}{k^2} + \left(\frac{1}{2} - a\right)^2 \right) + \left(\frac{1}{2} - F\right)\left(\frac{1}{2} - a\right) - \frac{F}{k^2} - \left(\frac{1}{2} + a\right)\frac{G}{k} \right] \tag{16}$$

with no reference made to the previous, incorrect formula. Here a denotes the position of the pivot point measured from the mid-chord positive forward in terms of half-chords. The agreement with linear theory is quite good at lower frequencies but diminishes at higher frequencies. This is expected due to the deforming wake used in the panel code, however, note that UPOT predicts a lower C_t than linear theory here, in contrast with the plunging case. Comparison with the experimental results show similar trends, but viscous effects dominate at low frequencies, explaining the much larger drag producing region in the experimental results. The poor comparison at higher frequencies brings into question the thrust measurement technique used in the experimental study.

In many experimental investigations, including Koochesfahani's, the drag or thrust generated by a body is predicted by measuring the momentum deficit

or surplus downstream of the body. Usually the assumptions are made that at the cross-section where velocities are measured the flow is parallel, the pressure is freestream, and the time-fluctuating quantities are small, resulting in the integral equation

$$T = \rho_\infty \int_{-\infty}^{+\infty} V(y)(V(y) - V_\infty)dy \ . \qquad (17)$$

If the velocity measurements are made sufficiently far downstream of the airfoil, such that the wake eddies are essentially diffused, then Eq. (17) yields reasonable results, but if the measurements are made in a region where the eddies are still coherent, then the assumptions will not hold. It is not clear from Koochesfahani's paper how far downstream the measurements were made for the thrust calculations included here in Fig. 12, but velocity profiles presented in his paper were made at one chordlength downstream of the trailing edge, and at that distance the eddies are still very much intact.

There is no diffusion in the panel code, so the vortex elements contain the same ideal vorticity for all time; therefore, the use of Eq. (17) in the panel code is of little scientific use. However, for academic purposes it is interesting to compare the predictions of the panel code using Eq. (17) with Koochesfahani's results. For a NACA 0012 pivoting about the quarter chord with $\Delta\alpha = 2$ degrees and $k = 20$, UPOT predicts a thrust coefficient of 0.13 (more than twice the value predicted by UPOT from surface pressure integration) compared to an interpolated value of 0.10 from Koochesfahani. The difference in these predictions is consistent with the viscous drag apparent in Koochesfahani's results at low reduced frequencies.

Comparable viscous calculations with the panel code are not possible in this case, as the chord Reynolds number (12,000) in Koochesfahani's experiments is far too low for the boundary layer method of UPOT.

The thrust coefficient is plotted as a function of k for several airfoils of varying thickness pitching about the leading edge with $\Delta\alpha = 2$ degrees in Fig. 13. Unlike the plunging case, airfoil thickness does influence thrust production for pitching airfoils, with the results approaching linear theory for thinner airfoils. This is consistent with flutter analysis presented in Ref. 14, where it was found that the flutter frequency increased for thicker airfoils. In Fig. 14 the thrust coefficient, power coefficient and propulsive efficiency are plotted for the pitching airfoil of Fig. 12. Note here that the maximum efficiency is only about 30 percent, and this occurs at a very low thrust coefficient, thus when viscous effects are considered, the efficiency will drop considerably.

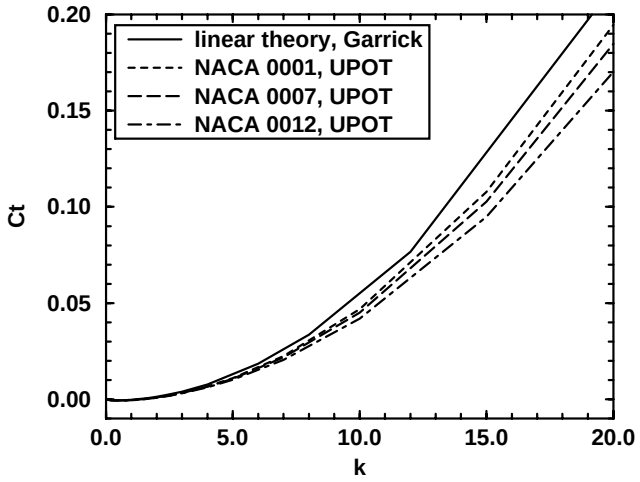

Fig. 13: Effect of airfoil thickness on C_t.

The negative efficiency values at low k are due to drag production for k less than about 2. Pivoting about the quarter chord, the power coefficient is always positive. This is in agreement with aeroelastic analysis which predicts that flutter will not occur with the pivot (or elastic axis) located at $c/4$.

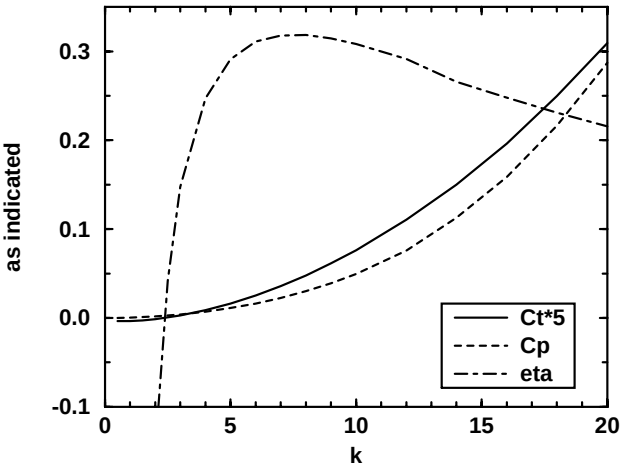

Fig. 14: Thrust, power and efficiency predictions.

Dual Mode With combined pitching and plunging motions the parameter space becomes quite large. In addition to variations of h, $\Delta\alpha$ and k, the phase, ϕ, between pitching and plunging is introduced, and there are additional interactions between the parameters. For example, by varying the ratio of hk and $\Delta\alpha$ the effective angle of attack, α_e, may change sign, where α_g is the geometric angle of attack and α_e is the angle of attack actually seen by the airfoil, as shown in Fig. 15.

In Fig. 16 the effect of these terms is perhaps more easily understood. In Fig. 16a the airfoil is only plunging (with the curved line representing the path

of the airfoil through the fluid), and while the airfoil always has a zero geometric angle of attack, it clearly has a sinusoidal effective angle of attack.

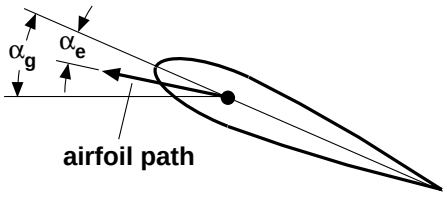

Fig. 15: Effective versus geometric angle of attack.

In Fig. 16b the airfoil is only pitching, and the effective and geometric angles of attack are equal. In Fig. 16c the foil is both pitching and plunging with $\phi = 90$, and while the geometric angle of attack is varying, the effective angle of attack is zero. In this case the influence of the airfoil on the fluid is quite small (but not zero, as the pitch rate and acceleration of the foil still create disturbances). In Figs. 16d and 16e the motion of Fig. 16c is duplicated but with smaller and larger pitch amplitudes, respectively, resulting in a sign change of the effective angle of attack. As will be shown, this is the key to thrust production or power extraction.

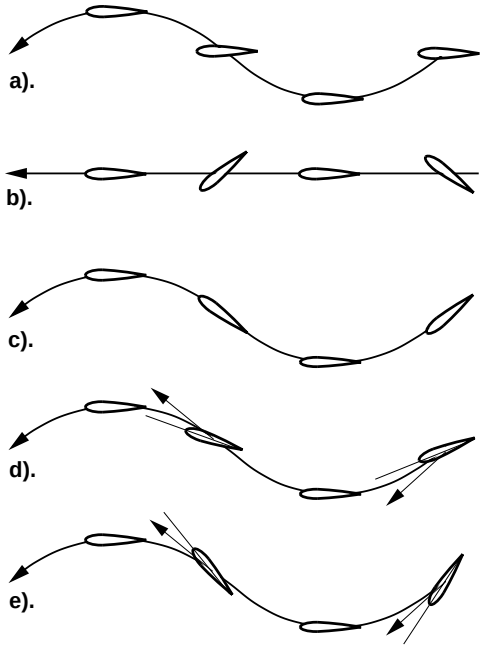

Fig. 16: Effective versus geometric angle of attack.

In Fig. 17 the propulsive efficiency is plotted as a function of the pitch amplitude for a NACA 0012 airfoil pitching about its quarter chord with a plunge amplitude of 0.2 and $\phi = 90$ degrees for several frequencies. It can be seen that for small pitch amplitudes (corresponding to Fig. 16d) thrust is produced, but at some pitch amplitude η is discontinuous, and at higher pitch amplitudes (corresponding to Fig. 16e) drag is produced and power is extracted from the flow. This is apparent for all k, but as k is increased the $\Delta\alpha$ where the discontinuity occurs increases.

The discontinuities correspond well with Fig. 16c, that is, the induced angle of attack due to the plunging motion is roughly equal to the geometric angle of attack at the discontinuity. For example, at $k = 1$, the induced angle of attack is $\alpha_i = \arctan(hk) = 11.3$ degrees, and the geometric angle of attack at the discontinuity is ≈ 11.5 degrees. Note that the peak efficiency for thrust production decreases with increasing frequency, and similarly the peak efficiency for power extraction increases (decreases in effectiveness as a windmill) for increasing frequency.

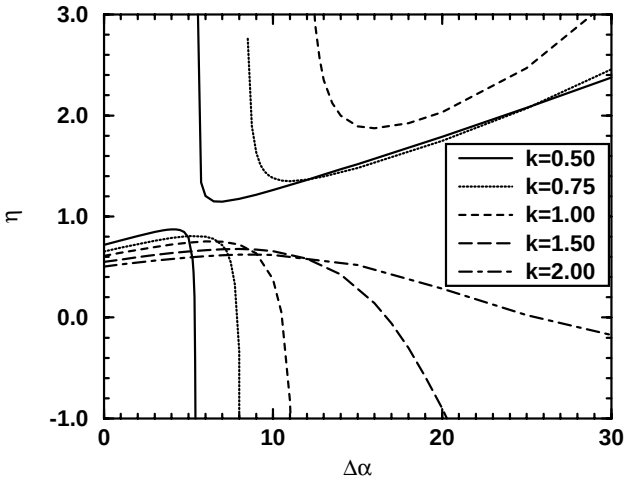

Fig. 17: Propulsive efficiency versus k and $\Delta\alpha$.

In Fig. 18 the frequency is fixed at $k = 0.5$ (resulting in $St = 0.1$) and the phase is varied, again with η plotted as a function of the pitch amplitude.

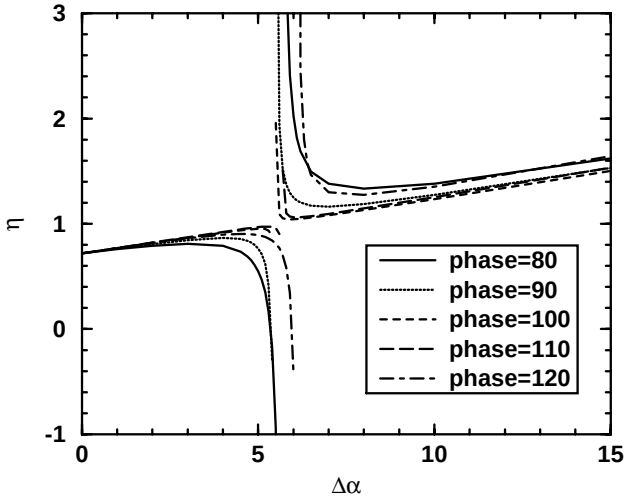

Fig. 18: Propulsive efficiency versus ϕ and $\Delta\alpha$.

The curves are similar in nature to the curves in Fig. 17, but it is apparent that optimal efficiency for both thrust production and power extraction at these conditions is reached at a greater phase angle than 90 degrees; around 107 degrees. As the optimal phase is approached the two branches of the plots, which resemble the branches of hyperbolas, seem to asymptotically approach a limiting line with a singularity at $\eta = 1$.

There is an important feature that does not show up in Figs. 17 and 18, and that is the relationship between C_t and η. In Fig. 19a, C_t, C_p and η are plotted as functions of ϕ for the NACA 0012, with $k = 0.5$, $h = 0.2$ (resulting in $St = 0.1$) and $\Delta\alpha = 4$ degrees.

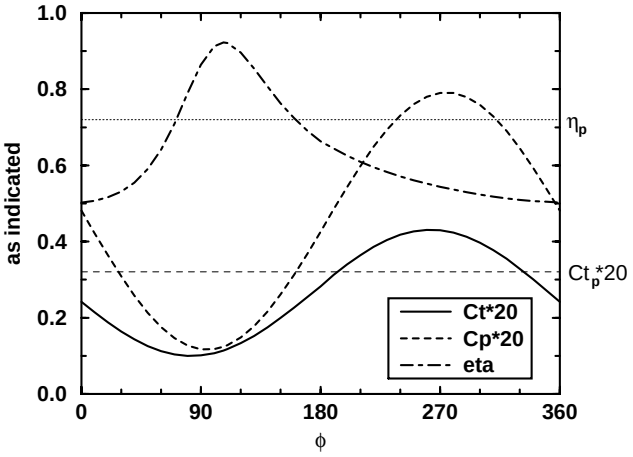

Fig. 19a: Dependence of C_t, C_p and η on ϕ.

It is clear from the plot that the phase for maximum efficiency nearly coincides with the phase for minimum C_t and C_p. This is unfortunate, because when the effects of viscosity are included, the values of C_t drop substantially, reducing η similarly. Also included on the plot and labeled on the right boundary of the plot are the C_t and η values obtained for a pure plunging motion with the same k and h. A greater efficiency is achieved for $70° < \phi < 160°$, however, C_t is greatly reduced from the plunge-only case over this entire range.

As shown previously in Fig. 11b, for an airfoil plunging with a constant Strouhal number better performance was obtained with lower k and higher h. In Fig. 19b similar data is shown for an airfoil pitching and plunging with $St = 0.1$, $\phi = 90$ degrees and $\Delta\alpha = 4$ degrees. Here again the propulsive efficiency increases asymptotically to unity as k is reduced to zero; however, now the thrust coefficient reaches a minimum value at a moderate frequency and then increases at higher frequencies.

Similar results to Fig. 19a are shown in Fig. 20, but with a pitch amplitude of 8 degrees.

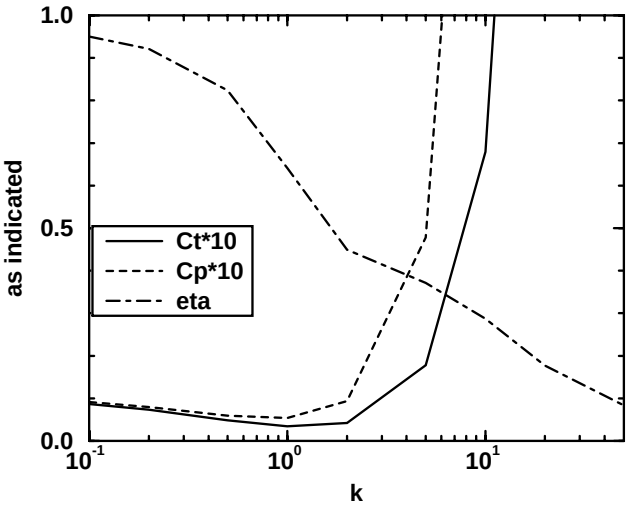

Fig. 19b: Thrust performance for constant $St = 0.1$.

With this larger pitch amplitude it is possible to generate thrust for some phase angles and extract energy from the flow for others. Both the C_t and C_p curves have a greater magnitude than in Fig. 19, such that they each have negative values over part of the phase spectrum. The optimum phase angle for these conditions is around 100 degrees, in approximate agreement with the experimental findings of McKinney and DeLaurier.[15]

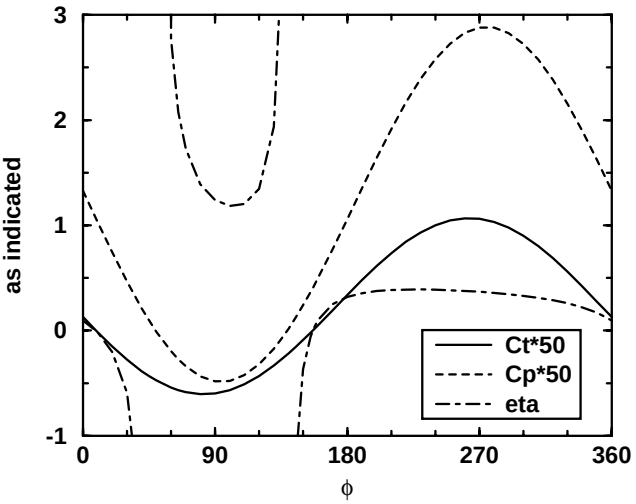

Fig. 20: Dependence of C_t, C_p and η on ϕ.

As previously mentioned, in the case of flapping-wing propulsion the point of maximum propulsive efficiency nearly coincides with the point of minimum thrust production, an unfortunate coincidence when the effects of viscosity are considered. However, for the case of power extraction from the flow, the point of optimum power-extraction efficiency nearly coincides with the point of maximum power extraction. This makes the use of flapping airfoils for power generation

appear very attractive; perhaps offering a more ecologically sound alternative to conventional hydroelectric turbines, One can imagine situating large flapping-wing generators in rivers under existing bridges. The flapping-wing generators would not require a dam and would consequently not restrict the passage of fish and boats.

For perspective a few examples are included here. For the optimal thrust conditions shown in Fig. 19a ($k = 0.5$, $h = 0.2$, $St = 0.1$, $\Delta\alpha = 4$ degrees, $\phi = 107$ degrees, $C_t = 0.0057$ and $C_p = 0.0062$), a generic wing with a $1m$ chord and $10m$ span, traveling at a freestream speed of $45m/s$ ($\approx 100mph$) in sea-level air would result in a thrust force of about $71N$ ($\approx 16lbs$) and would require about $3500W$ ($\approx 4.7hp$) to operate. The same wing in water traveling at a freestream speed of $10m/s$ ($\approx$ 20 knots) would produce about $2900N$ ($640lbs$) of thrust and require about $31,000W$ ($\approx 42hp$) to operate.

For the optimal power extraction conditions used in Fig. 20 ($k = 0.5$, $h = 0.2$, $St = 0.1$, $\Delta\alpha = 8$ degrees, $\phi = 100$ degrees and $C_p = -.0096$)and the same generic wing used as a windmill, in sea-level air with a wind speed of $10m/s$ ($\approx 22mph$) roughly $60W$ would be extracted. In water with a stream speed of $4.5m/s$ ($\approx 10mph$) roughly $4400W$ would be extracted.

Note, the thrust produced increases with U_∞^2, but the power required/generated increases with U_∞^3; thus, for propulsion it is advantageous to minimize the freestream speed, and for power extraction the opposite is true. Also note that the mass/inertia of the wing and all viscous and mechanical losses are ignored. For flapping-wing flight it may be possible to overcome most of the inertial energy requirements needed to accelerate the mass of the wing sinusoidally using a spring. In fact, it is likely that flying insects employ such a spring according to Alexander.[40]

As previously mentioned, it has been theorized that maximum efficiency will occur when the velocity profile downstream of the flapping foil most closely resembles the rectangular velocity profile downstream of an actuator disk. In Fig. 21 the velocity profiles at several stations in the wake of the NACA 0012 plunging with $k = 0.5$, $h = 0.2$, $St = 0.1$ and zero angle of attack are plotted (results for this case were previously plotted in Figs. 9 and 19a). The x/c measurements are the distance between the foil leading edge and the measured velocity profile. The width of the jet-like profile quickly expands downstream. At $x/c = 15$, 14 chordlengths downstream of the trailing edge (just over one wake wavelength), the jet-profile is almost 5 times wider than at the trailing edge. The case shown has a computed efficiency of 72 percent and a thrust coefficient of 0.016.

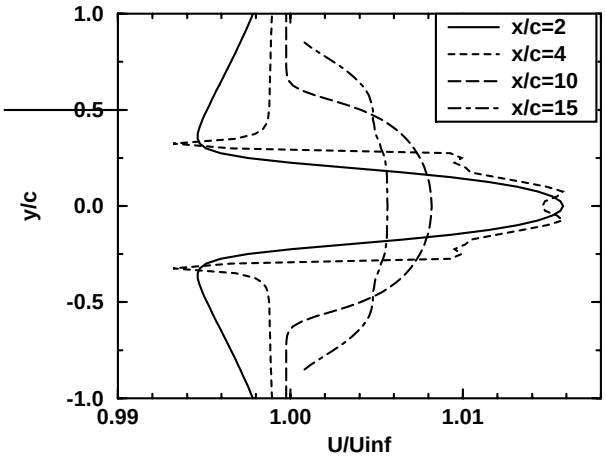

Fig. 21: Wake velocity profiles for plunging-only.

In Fig. 22 similar data is shown, but for a pitching and plunging foil at near optimum conditions with $k = 0.5$, $h = 0.2$, $St = 0.1$, $\Delta\alpha = 4$ degrees, $x_p = 0.25$ and $\phi = 110$ degrees (results for this case were previously plotted in Figs. 17-19). Here the efficiency is about 92 percent but the thrust coefficient is just 0.0059. The jet-profile resembles the ideal actuator-disk profile much more closely and remains more *focused* far downstream.

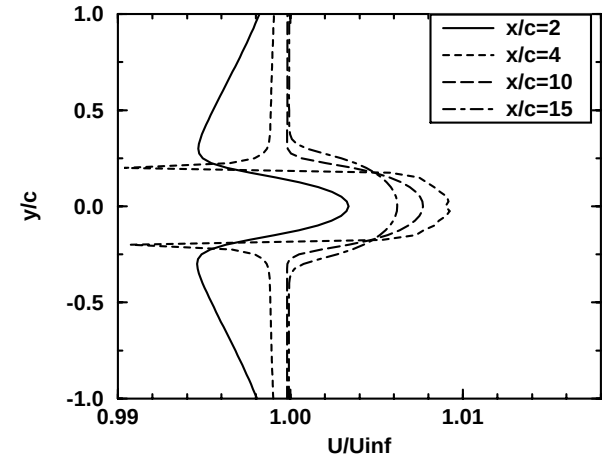

Fig. 22: Wake velocity profiles for dual-mode motion.

It would be instructive to recompute all of the presented data with the inclusion of profile drag. That will have to be reserved for a future publication, but a sample case is included here to demonstrate the capabilities of the hybrid code. In Fig. 23 a NACA 0012 is plunged with $h = 0.1$ at a chord-Reynolds number of 10^6, and the computed C_t is plotted as a function of k. For comparison, the inviscid curve and the theoretical curve predicted by Garrick are included. For the conditions considered here, the inclusion of profile drag has the effect of shifting the C_t values by roughly a constant value.

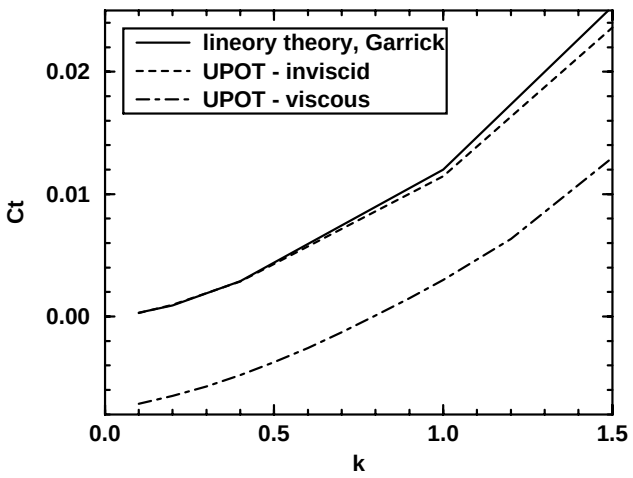

Fig. 23: Thrust with profile drag.

The reduction in C_t, and especially the change in sign, alters the resultant propulsive efficiency dramatically, as shown in Fig. 24. For k less than about 0.8, where C_t is negative, η is also negative but approaches the inviscid solution at higher frequencies.

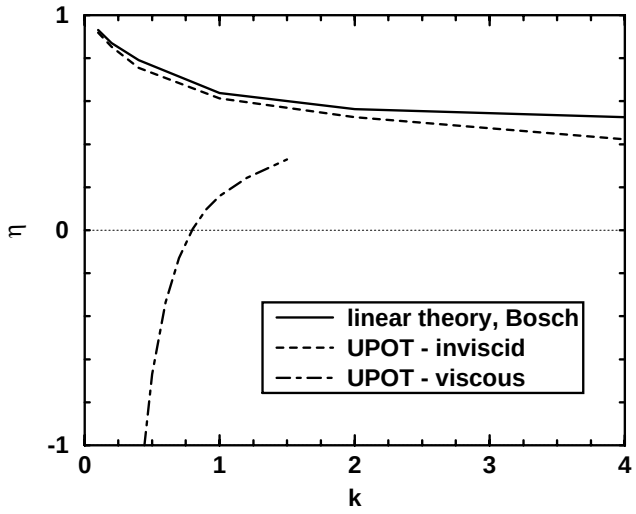

Fig. 24: Propulsive efficiency with profile drag.

The present numerical approach does not allow viscous solutions at high frequencies or large effective angles of attack, but the roughly linear shift in the C_t plot in Fig. 23 suggests that reasonable results may be obtained by extrapolating the linear shift to higher frequencies. Previous experimental results indicated that flow separation may be significant for St greater than about 1,[7] so that should serve as an upper limit for the extrapolation.

Flapping Wing in Ground Effect Observations of birds flying low over water suggest that there may be significant performance advantages to flapping-wing flight near a ground plane, as there is with fixed-wing flight. Recall from potential-flow theory that a steady, two-dimensional lifting airfoil in a uniform flow near a ground plane encounters a thrust force due to the circulation about the *image* airfoil. A similar thrust force may result in the unsteady case due to the proximity of the *image* wake.

Here the two-foil code is used to model ground-effect flight as previously illustrated in Fig. 6c. In Fig. 25 the propulsive efficiency is plotted as a function of the distance from the ground-plane, h_g, for a NACA 0012 at $\alpha = 0$, plunging with $h = 0.2$ and with varying reduced frequency.

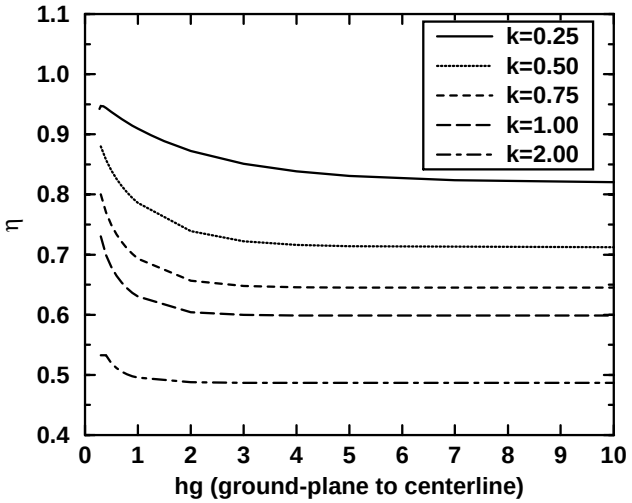

Fig. 25: Propulsive efficiency near a ground plane.

It is clear that the propulsive efficiency increases dramatically as h_g is reduced. As h_g is increased, η asymptotically approaches the single foil results previously shown in Fig. 8. At lower frequencies the beneficial effects are felt for several chord lengths away from the wall, but at larger frequencies the effect is lost within a single chord length separation from the ground-plane.

Conclusions

Numerical methods were described for the systematic computation of unsteady, inviscid, incompressible, two-dimensional flows about moving airfoils or airfoil combinations. Additionally a boundary layer algorithm was described capable of predicting profile drag on these unsteady airfoils. The single foil code, accompanied by a GUI front-end, provided flow visualization and flow measurement techniques similar to those available in experimental facilities. Both unsteady codes were used to investigate flapping-wing propulsion and power-extraction.

Results for single mode (pitching or plunging) motions agree well with linear theory for low frequen-

cies and amplitudes, as expected, but show additional losses at conditions were non-linearities become significant. It was found that at Strouhal numbers greater than roughly 1 the non-linear wake losses symmetry, deflecting away from the centerline, resulting in both an average thrust and an average lift. Investigations of the effect of wake non-linearity showed that computed wake deformation was responsible for most of the difference between linear theory and the present approach. It was shown that the propulsive efficiency of plunging airfoils could be greatly increased by decreasing the reduced frequency and increasing the amplitude while holding the Strouhal number constant.

Increases in propulsive efficiency were demonstrated with dual-mode motions (combined pitching and plunging) with simultaneous decreases in the thrust coefficient. It was consistently found that the conditions for maximum propulsive efficiency nearly coincided with the conditions for minimum thrust coefficient; an unfortunate condition when flow viscosity is considered. While quasi-steady theory predicts optimal thrust production with pitch and plunge motions 90 degrees out of phase, it was found that for higher frequencies the optimal phase shift increases. Additionally, it was observed that the jet-profile generated by the flapping foil approaches the ideal, square profile of an actuator disk at conditions yielding high propulsive efficiencies, and the velocity profile remained focused far downstream. This observation may be of little use, however, since the computed, inviscid thrust in these conditions reduced to near zero.

If the pitch-amplitude of a dual-mode flapping wing is increased sufficiently it was found that drag was produced and power was extracted from the airfoil, a condition that would lead to flutter of a free airfoil. For this to occur the pitch amplitude must exceed the induced angle of attack due to the plunging motion, and the phase between pitch and plunge is restricted to a range near 90 degrees. It was shown that the conditions leading to optimum power extraction nearly coincide with the conditions for maximum power extraction, suggesting that flapping wings may be suitable for windmill or watermill power generation applications.

The inclusion of profile drag results in a nearly linear reduction in thrust in the frequency range analyzed. Consequently, very rapid results of reasonable accuracy may be obtainable using simple modeling and extrapolation techniques.

The effect of flapping-wing flight near a groundplane was investigated using the two-airfoil code and potential-flow image theory. It was shown that propulsive efficiencies increase dramatically near a groundplane, but that at higher frequencies the beneficial effect diminishes rapidly as the foil is moved away from the wall.

Acknowledgments

This investigation was partially supported by the Naval Postgraduate School National Research Council Fellowship Program (KDJ) and the Office of Naval Research (MFP).

References

[1] Knoller, R., "Die Gesetze des Luftwiderstandes," **Flug- und Motortechnik (Wien)**, Vol. 3, No. 21, 1909, pp. 1-7.

[2] Betz, A., "Ein Beitrag zur Erklärung des Segelfluges," **Zeitschrift für Flugtechnik und Motorluftschiffahrt**, Vol. 3, Jan. 1912, pp. 269-272.

[3] Katzmayr, R., "Effect of Periodic Changes of Angle of Attack on Behavior of Airfoils," NACA Report No. 147, Oct., 1922. (translated from **Zeitschrift für Flugtechnik und Motorluftschiffahrt**, March 31, pp. 80-82, and April 13, 1922, pp. 95-101).

[4] Birnbaum, W., "Das ebene Problem des schlagenden Flüels," **Zeitschrift für Angewandte Mathematik und Mechanik**, Vol. 4, No. 4, Aug., 1924, pp. 277-292.

[5] Birnbaum, W., "Der Schlagflügelpropeller und die kleinen Schwingungen elastisch befestigter Tragflügel," **Zeitschrift für Flugtechnik und Motorluftschiffahrt**, Vol. 15, 1925, pp. 128-134.

[6] Von Kármán, T. and Burgers, J. M., "General Aerodynamic Theory - Perfect Fluids," Division E, Vol. II, Aerodynamic Theory, Ed. Durand, W. F., 1943, p. 308.

[7] Jones, K. D., Dohring, C. M. and Platzer, M. P., "Wake Structures Behind Plunging Airfoils: A Comparison of Numerical and Experimental Results," AIAA Paper No. 96-0078, Jan., 1996.

[8] Garrick, I. E., "Propulsion of a Flapping and Oscillating Airfoil," NACA Report 567, 1936.

[9] Theodorsen, T., "General Theory of Aerodynamic Instability and the Mechanism of Flutter," NACA Report No. 496, 1935.

[10] Schmidt, W., "Der Wellpropeller, ein neuer Antrieb fuer Wasser-, Land-, und Luftfahrzeuge," Z. Flugwiss. Vol. 13, 1965, pp. 472-479.

[11] Bosch, H., "Interfering Airfoils in Two-dimensional Unsteady Incompressible Flow," AGARD CP-227, Paper No. 7, Sept. 1977.

[12] DeLaurier, J. D. and Harris, J. M., "Experimental Study of Oscillating-Wing Propulsion," **Journal of Aircraft**, Vol. 19, No. 5, May, 1982, pp. 368-373.

[13] Koochesfahani, M. M., "Vortical Patterns in the Wake of an Oscillating Airfoil," **AIAA Journal**, Vol. 27, No. 9, Sept. 1989.

[14] Jones, K. D. and Platzer, M. F., "Time-Domain Analysis of Low-Speed Airfoil Flutter," **AIAA Journal**, Vol. 34, No. 5, May 1996.

[15] McKinney, W. and DeLaurier, J., "The Wingmill: A Oscillating Wing Windmill," Journal of Energy, Vol. 5, No. 2, Mar.-Apr., 1981, pp. 109-115.

[16] Liu, P., "Three-Dimensional Oscillating Foil Propulsion," Masters Engineering Thesis, University of Newfoundland, march, 1991.

[17] Liu, P., "A Time-Domain Panel Method for Oscillating Propulsors with Both Chordwise and Spanwise Flexibility," Ph.D. Thesis, University of Newfoundland, 1996.

[18] Send, W., "The Mean Power of Forces and Moments in Unsteady Aerodynamics," **Zeitschrift für Angewandte Mathematik und Mechanik**, Vol. 72, 1992, pp. 113-132.

[19] Send, W., "Otto Lilienthal und der Mechanismus des Schwingenflugs," DGLR-JT96-030, German Aerospace Congress, Dresden, Sept., 1996.

[20] Teng, N. H., "The Development of a Computer Code for the Numerical Solution of Unsteady, Inviscid and Incompressible Flow over an Airfoil," Master's Thesis, Naval Postgraduate School, Monterey, CA, June 1987.

[21] Jones, K. D. and Center, K. B., "Numerical Wake Visualization for Airfoils Undergoing Forced and Aeroelastic Motions," AIAA Paper No. 96-0055, Jan., 1996.

[22] Hess, J. L. and Smith, A. M. O., "Calculation of Potential Flow about Arbitrary Bodies," **Progress in Aeronautical Sciences**, Vol. 8, pp. 1-138, Pergamon Press, Oxford, 1966.

[23] Basu, B. C. and Hancock, G. J., "The Unsteady Motion of a Two-Dimensional Aerofoil in Incompressible Inviscid Flow," **Journal of Fluid Mechanics**, Vol. 87, 1978, pp. 159-168.

[24] Neace, K. S., "A Computational and Experimental Investigation of the Propulsive and Lifting Characteristics of Oscillating Airfoils and Airfoil Combinations in Incompressible Flow," Master's Thesis, Dept. of Aeronautics and Astronautics, Naval Postgraduate School, Monterey, CA, Sept. 1992.

[25] Platzer, M. F., Neace, K. S. and Pang, C. K., "Aerodynamic Analysis of Flapping Wing Propulsion," AIAA Paper No. 93-0484, Jan. 1993.

[26] Tuncer, I. H., Platzer, M. F. and Ekaterinaris, J. A., "Computational Analysis of Flapping Airfoil Aerodynamics," ASME Fluids Engineering Division, Summer Meeting, June, 1994.

[27] Riester, P. J., "A Computational and Experimental Investigation of Incompressible Oscillatory Airfoil Flow and Flutter Problems," Master's Thesis, Naval Postgraduate School, Monterey, CA, June 1993.

[28] Turner, M., "A Computational Investigation of Wake-Induced Airfoil Flutter in Incompressible Flow and Active Flutter Control," Master's Thesis, Naval Postgraduate School, Monterey, CA, March, 1994.

[29] Keller, H. B. and Cebeci, T., "Accurate Numerical Methods for Boundary-Layer Flows, pt. 2, Two-Dimensional Turbulent Flows," **AIAA Journal**, Vol. 10, p. 1193, 1972.

[30] Nowak, L. M., "Computational Investigations of a NACA 0012 Airfoil in Low Reynolds Number Flows," Master's Thesis, Naval Postgraduate School, Monterey, CA, Sept., 1992.

[31] Cebeci, T., "Essential Ingredients of a Method for Low Reynolds-Number Airfoils," **AIAA Journal**, Vol. 27, No. 12, Dec., 1989, pp. 1680-1688.

[32] Cebeci, T. and Smith, A. M. O., "Calculation of Profile Drag of Airfoils at Low Mach Numbers," **Journal of Aircraft**, Vol. 5, No. 6, Nov.-Dec., 1968, pp. 535-542.

[33] Abbott, I. H. and von Doenhoff, A. E., Theory of Wing Sections, Dover, New York, June 1958.

[34] Pang, C. K., "A Computer Code for Unsteady Incompressible Flow past Two Airfoils," Aeronautical Engineer's Thesis, Dept. of Aeronautics and Astronautics, Naval Postgraduate School, Monterey, CA, Sept. 1988.

[35] Triantafyllou, G. S., Triantafyllou, M. S. and Grosenbaugh, M. A., "Optimal Thrust Development in Oscillating Foils with Application to Fish Propulsion," **Journal of Fluids and Structures**, Vol. 7, 1993, pp. 205-224.

[36] Ohashi, H. and Ishikawa, N., "Visualization Study of a Flow Near the Trailing Edge of an Oscillating Airfoil," Bulletin of the Japanese Society of Mechanical Engineers, Vol. 15, 1972, pp. 840-845.

[37] Kadlec, R. A. and Davis, S. S., "Visualization of Quasiperiodic Flows," **AIAA Journal**, Vol. 17, 1979, pp. 1164-1169.

[38] Triantafyllou, M. S. and Triantafyllou, G. S., "An Efficient Swimming Machine," **Scientific American**, March, 1995, pp. 64-70.

[39] Garrick, I. E., "Nonsteady Wing Characteristics," Division F., Vol. VII High Speed Aerodynamics and Jet Propulsion; Aerodynamic Components of Aircraft at High Speeds, Eds. Donovan, A. F. and Lawrence, H. R., Princeton University Press, Princeton, NJ, 1957, pp. 658-793.

[40] Alexander, R. M., "Springs for Wings," **Science**, Vol. 268, April 7, 1995, pp. 50-51.

[41] Hall, K. C. and Hall, S. R., "Minimum Induced Power Requirements for Flapping Flight," **Journal of Fluid Mechanics**, Vol. 323, Sept., 1996, pp. 285-315.